Temporal and spatial variability of vertical salt flux in a highly stratified estuary.

Daniel G. MacDonald[1] and Alexander R. Horner-Devine[2]

[1]Department of Estuarine and Ocean Sciences
School for Marine Science and Technology
University of Massachusetts Dartmouth
and
University of Massachusetts School of Marine Sciences

[2]Department of Civil and Environmental Engineering
University of Washington

Submitted to *Journal of Geophysical Research: Oceans*
November 1, 2007

Corresponding author information:

Daniel G. MacDonald
Department of Estuarine and Ocean Sciences
School for Marine Science and Technology
University of Massachusetts Dartmouth
706 South Rodney French Boulevard
New Bedford, MA 02744-1221

email: dmacdonald@umassd.edu
phone: (508) 910-6334
fax: (508) 910-6371

ABSTRACT

The temporal and spatial variability of vertical salt flux in the dynamics of the Fraser River Estuary, British Columbia, was investigated observationally, using several different direct and indirect indicators of buoyancy flux. Data were collected from the estuary using shipboard instrumentation, primarily an acoustic Doppler current profiler (ADCP), and a towed conductivity, temperature, depth (CTD) unit. Direct estimates of buoyancy flux were made from along channel control volume analyses and from measurements of overturn scales in the vertical salinity profiles. The spatial and temporal evolution of the salt wedge structure through a tidal cycle was evaluated using the results of these buoyancy flux calculations, as well as gradient Richardson number, Froude number, and stratification profiles. Vertical salt flux, as opposed to seaward advection of high salinity fluid, was found to be the dominant mechanism responsible for removal of salt from the estuarine channel during each daily tidal cycle. Buoyancy flux was highly variable in time and space, however, with vertical salt flux during ebb tides on the order of 2 to 3 times greater than that estimated during floods. This is due to an increase in vertical velocity shear and a sharp increase in stratification, which was found to occur during early ebb. Mixing during all phases of the tide was considered significant, however. Enhanced mixing was observed spatially within a region dominated by a channel constriction in which the channel narrows by approximately 25%.

1.0 Introduction

Estuaries are an important component of the coastal ocean, providing nutrient-rich waters that form the foundation of fertile and productive ecosystems. In the coastal ocean, estuaries continue to play an important role, with a significant impact on the distribution of land-derived nutrients, contaminants and sediment. These far field distributions are driven to a large extent by localized mixing processes within an estuarine channel, where the confluence of energy from river and tidal sources can generate sufficient turbulence to overcome local stratification. Early studies of estuarine physics (e.g., Schijf and Schonfeld, 1953; Pritchard, 1952, 1954, 1956) recognized estuarine mixing as an important component of estuarine circulation. However, even today, attempts to quantify mixing rates continue to present a major technical challenge.

Mixing in estuaries can be highly variable, dependent on diurnal and fortnightly variations in tides, seasonal cycles of river discharge and variations in channel topography. Simpson et al. (1990) found that in the partially mixed estuary of Liverpool Bay, intense mixing occurs primarily near the end of the flood, particularly near spring tides. Measurements of mixing in the Hudson River Estuary (Peters, 1999), another partially mixed estuary, indicate that about 30% of the total fortnightly vertical salt flux occurs during spring ebbs, with the majority of the remainder provided during floods throughout the fortnightly cycle. A recent numerical study of mixing in a partially mixed estuary (MacCready and Geyer, 2001) indicates that mixing is most intense during the peak ebb, but more vertical salt flux occurs during the peak flood due to an extended along-channel length of the isopycnals. In the Tacoma Narrows section of Puget Sound, a large fjord-like estuary, channel curvature and the flow dynamics over a sill were found to produce strong vertical mixing (Seim and Gregg, 1997), reiterating the often observed

importance of topographic features to mixing processes (e.g., Geyer and Canon, 1982; Farmer and Armi, 1999; Wesson and Gregg, 1994).

While significant progress has been made in identifying mixing in different estuarine environments, fundamental questions still remain regarding the mechanisms responsible for mixing such as where and when the mixing actually occurs, and how these processes are dynamically controlled. This paper focuses on measurements from the Fraser River (British Columbia) estuary, a highly stratified estuary characterized by a tidally oscillating salt wedge. Such estuaries, in particular, have not been well characterized, as a majority of the existing studies have focused on partially mixed estuaries, such as the Hudson river (e.g. Trowbridge et al 2001) Although high stratification can provide an increased resistance to mixing it may also result in more productive vertical salt flux once local turbulence is energetic enough to overcome the stratification.

The Fraser River estuary is a highly energetic salt wedge estuary, characterized by a strongly diurnal tide, with amplitudes exceeding 4 m during spring tides, and a river discharge that can peak at over 10,000 m^3s^{-1} during the summer freshet. These conditions combine to generate a salt wedge that advances into the channel 15 to 20 km landward of the mouth during the flood portion of every tidal cycle, retreating to the mouth once a day during the larger of the two daily ebbs. Several previous studies have described the mixing climate of the Fraser River estuary (e.g. Geyer and Smith, 1987; Geyer, 1988; Geyer and Farmer, 1989). These studies have suggested that mixing is more prominent in the Fraser during ebbs, and at localized constrictions in the channel width (Geyer, 1985), but no attempts to directly assess mixing rates within the estuary were attempted. It is still unclear to what degree mixing on the flood is significant in natural salt-wedge systems, and, specifically with regards to the Fraser River Estuary, how much

mixing actually occurs during a typical tidal cycle, and where and when that mixing is most intense.

The objectives of understanding the dynamics of estuarine circulation within the channel are addressed in this paper by focusing on the key processes of shear induced mixing, the straining of isopycnals by velocity shear, and advection. The interaction of these processes is responsible for setting and maintaining the degree of stratification within the estuary. A specific goal of the work is to address temporal variations in stratification and diapycnal mixing through the tidal cycle, particularly the relative strength of mixing on both the flood and ebb portions of the tidal cycle. A second goal is to determine the dominant processes responsible for the evacuation of salt from the channel during the ebb; that is, horizontal advection driven by tidal oscillation, or vertical mixing and subsequent transport in the upper water column. Spatial variations in mixing intensity are also evaluated, both with respect to their importance to the temporal variability, and to previous observations of localized mixing events at channel constrictions (e.g. Geyer, 1985).

2.0 Study Description

The data utilized in this study were collected between June 30 and July 4, 2000, within the Fraser River Estuary. This sampling period was centered on the spring tide, which occurred on July 2nd, with a tidal amplitude of 4.7 m, and was characterized by river discharges on the order of 7,000 m^3s^{-1}. The analyses described here often rely on the assumption that the dynamics of the salt wedge are similar across all sampling days, which is justified based on the small observed variations in tidal amplitude (0.2 m or less for four of the five sampling days, with a tidal amplitude approximately 0.7 m less than the peak on June 30) and river discharge (total discharge increased from approximately 6500 to approximately 7200 m^3/s across the five day

sampling period). .

Data were collected from shipboard instrumentation, primarily two hull-mounted Acoustic Doppler Current Profilers (ADCPs), operating at 1200 kHz and 300 kHz, and a towed Ocean Sensors 200 Series conductivity, temperature, depth (CTD) unit. The lower 18 km of the channel are shown in Figure 1. Data were collected primarily at an anchor station located approximately 3.4 km landward of Sand Heads, shown by the black triangle in Figure 1, and from channel operations landward of the anchor station.

As an example of the structure of the salt wedge, two composite profiles of the salt wedge, compiled from data collected during the ebb from four days of operations in the channel, are shown in Figure 2. The earlier of the two profiles (2.3 hours after high tide) represents a portion of the salt wedge, from the anchor station location landward to the entrance of Steveston Harbor, but does not include the head of the salt wedge (Figure 2a). The second profile represents conditions 1 hour later and extends from the anchor station location landward past the head of the salt wedge, which was located approximately 10.5 km from the mouth (Figure 2b). In both profiles it is clear that the salt wedge is very strongly stratified, with salty bottom water often separated from fresh surface water by an interface that is only a few meters thick.

2.1 Time series data

Data were collected from the anchor station through a complete tidal cycle on July 3rd and 4th. A CTD cast was performed approximately every 15 minutes, with both ADCPs running continuously, providing good temporal resolution across the 18 hour period during which the presence of salt was observed. Tidal stage during the anchored period is plotted with near-surface and near-bottom velocities in Figure 3. For convenience in comparing data from different days, all times are referenced to the high tide leading the larger of the two daily ebbs.

The conditions and salinity structure observed at the anchor station location through the time series are shown in Figure 4. Well mixed regions forming the bulk of the upper and lower layers are separated by a pycnocline, which varies in position and intensity through the tidal cycle. The velocity structure is strongly baroclinic during almost the entire tidal cycle, with the location of the velocity reversal varying between 7 and 13 m above the bottom. Only during the second, stronger, ebb does the entire water column flow uniformly seaward. Note that the hatched region in Figure 4 represents the region of positive velocity shear. Within this region, velocities increase in the landward direction moving away from the channel bed. Geyer and Farmer (1989) suggest that shear is most intense, and mixing most active at times when no such region exists, so that the bottom shear and interfacial shear act in unison.

2.2 Channel Transects

Data were collected during the second ebb from a series of cross-channel CTD "fences", typically consisting of three to four CTD stations coupled with ADCP velocity data. A circuit consisting of multiple fences was sampled repeatedly during the course of the observation period. All measurements were taken during the largest daily ebb on July 1st, 2nd, and 3rd, and were located between the anchor station discussed above and the entrance to Steveston Harbor, approximately 8.7 km landward of Sand Heads.

3.0 Analysis Techniques

A variety of analysis techniques were used to interpret the time series and channel transect data sets, as described in the following sections.

3.1 Control Volume Analyses

Turbulence calculations were performed for both the time series and channel data using a variation of the control volume technique first described by MacDonald and Geyer (2004) and

subsequently utilized for a variety of estuarine and plume flows (e.g. Chen and MacDonald 2006; MacDonald et al 2007).

In the case of the time series data, mean buoyancy flux is estimated for the entire tidal cycle. The conceptual limits of the control volume for this analysis extend from the anchor station location to a point beyond the landward extent of the salt wedge excursion. The time series data adequately constrains the salt balance as all salt must enter and exit the control volume at the anchor station location. Extending the limits of the analysis across the entire period that salt is present also eliminates the time dependent term.

A key difference between this application of the control volume technique, and that described by MacDonald and Geyer (2004) is that the volume balance cannot be constrained by the time series data, due to unknown freshwater velocities landward of the salt wedge. Thus, vertical profiles of the vertical advective velocity, $\overline{w}$, cannot be generated, and it must be assumed that $\overline{S'w'}$ is equivalent to $\overline{Sw}$, with the implication that $\overline{w}$ is zero. In fact, $\overline{w}$ must be exactly zero at the level of maximum $\overline{S'w'}$ (e.g. McDougall 1984). Furthermore, due to the change of sign of diahaline velocity through the water column, the assumption should also be reasonable with respect to averages taken in the vertical or across salinity space.

With these considerations, a salt equation for the time series control volume can be written as

$$\overline{S'w'}\left(\widetilde{S}\right) = \frac{\int_0^{z_{\widetilde{S}}} \int_{cycle} Subdtdz}{\int_{cycle} A_{SI}\, dt} \qquad (1)$$

where *S*, *u, b,* and $z_{\widetilde{S}}$ are the mean salinity, mean along channel velocity, cross-channel width, and the observed depth of the given isohaline, respectively. Given $\overline{S'w'}$ from (1), buoyancy flux

is estimated as $B = \frac{g}{\rho}\overline{\rho' w'} = g\beta\overline{S' w'}$, where g represents gravitational acceleration, ρ is density,

and $\beta = \frac{1}{\rho}\frac{\partial \rho}{\partial S} = 0.77 \times 10^{-3}$ psu^{-1}, for temperatures near 10^{o} C.

The projected area of a given isopycnal surface, represented as A_{SI} in the denominator of (1), requires an estimate of the landward extent of the salinity intrusion beyond the anchor station. This was accomplished by taking the difference between running integrals of inbound and outbound salt flux to identify the mass of salt present in the channel as a function of time. Combining this information with an observation of the location of the head of the salt wedge during an earlier tidal cycle allowed the length of the salinity intrusion to be estimated. To generate a time series of isopycnal area, a representative channel width of 700 m was applied to the time series of salt wedge length.

The control volume approach utilized in the upstream channel is consistent with the method described in MacDonald and Geyer (2004). Analysis of two adjacent fences (typically separated by a half to one kilometer) was conducted by summing fluxes in the cross channel direction assuming each station was representative of conditions across a specific width. This procedure resulted in the integration of any cross channel variability, allowing the volume and salt budgets to be constrained. Using this approach profiles of buoyancy flux across salinity space were generated for 15 locations in time and space. At each location, estimates were generated for each isopycnal between 1 and 28 psu, with a resolution of 1 psu.

In an attempt to account for the non-synoptic nature of the measurements, data from different locations used for a specific calculation were linearly interpolated to the same point in time prior to evaluation of the salt and volume balance terms. The magnitude of the total error for each control volume analysis, which can enter the calculations as a result of sampling

frequency and spatial heterogeneity, was assessed by determining if salt was balanced within each section. Observed errors were distributed linearly in z to close the salt balance, and force $\overline{S'w'}$ to zero at the channel bottom. In order to minimize the impact of these time-dependent errors, individual estimates of buoyancy flux were averaged across many realizations in time and/or space.

3.2 Overturn Analyses

Estimates of buoyancy flux were also generated from overturn scales, L_t, derived from CTD profiles, and assuming a turbulent Froude number of one, such that the overturn scale was assumed equal to the Ozmidov scale, $L_O = \left(\varepsilon / N^3\right)^{\frac{1}{2}}$ (Peters et al, 1988), where ε is the dissipation rate of TKE. This is a commonly used approach to estimating turbulent quantities (e.g. Ferron et al 1998; Orton and Jay 2005). Here we calculate buoyancy flux directly as $B_t = \left(\frac{Ri_f}{1 - Ri_f}\right) L_t^2 N^3$, where Ri_f is the flux Richardson number. Typical values of Ri_f are on the order of 0.2 (e.g. Ivey and Imberger 1991; MacDonald and Geyer 2004).

The overturn scale analysis utilized CTD data from casts performed between 3 km and 8 km from the mouth during the second ebb, including those utilized for the channel control volume calculations. Each individual CTD cast, resampled to 5 cm in the vertical, was sorted in order of increasing salinity, and compared with the original. A vertical offset was identified for each point as the smallest vertical displacement between an observed salinity, and the location of that salinity value within the sorted profile. The mean overturn scale for the cast was then taken as the rms value of all displacements (including 0, or non-displacements) within the cast. This method provided a natural scaling for stable regions of the water column, and proved a more effective method for identifying a mean cast overturn scale than averaging individual values of L_t

for each observed overturn (as described in Thorpe, 1977). The mean overturn scale for the cast was then combined with similar results from other casts to generate broader based estimates by averaging across time and space.

It should be noted that overturns are a transient and somewhat elusive phenomena. In order to generate an accurate representation of the nature of the turbulence within a region, a sufficiently large averaging window must be used. In the present data set, individual cast values were observed to vary significantly over short time periods. This is due to the probability of observing an overturn during any single cast, and furthermore, the state of roll-up or decay which might characterize a specific overturn at the moment of observation. In any turbulent field, there are a collection of simultaneous eddies at various stages of their evolution, and some portion of the field where no eddies exist at all, as discussed recently by MacDonald et al (2007). Thus, the aggregation of multiple casts is necessary to adequately resolve the field. For this reason, an overturn analysis of the time series data is not presented. CTD casts were performed approximately every 15 minutes during the time series, which did not provide a sufficient number of casts to adequately resolve the turbulent field at a high enough resolution to capture important transitions, such as those seen during the early portions of the final ebb.

3.3 Stratification

Some gauge of the stratification present in the estuary is crucial for putting other estimates of mixing and straining into context. Simpson et al. (1990) proposed that the degree of stratification in an estuary is established primarily by the interaction of two competing mechanisms: the stratifying effects of velocity-induced straining, and the homogenizing effects of shear-induced mixing. They quantified stratification by the amount of energy input needed to homogenize a vertical density profile. However, under highly stratified conditions, or in regions

of intense interfacial wave activity, this definition can be misleading as the required energy input changes depending on the vertical location of the layer interface relative to mid-depth.

Here, stratification will instead be gauged by a non-dimensional representation of mixed layer thickness:

$$\psi = \frac{1}{2}\frac{h}{L_{50}},\ L_{50} = z_{75} - z_{25} \qquad (2)$$

where h represents the local water column depth, and L_{50} represents the vertical distance between the 75th (z_{75})and 25th (z_{25}) percentiles of the system salinity range. In the Fraser system, where salinities typically range from 0 to 28 psu, L_{50} at any location is the vertical distance between the 7 and 21 psu isohalines. If neither of these isohalines is observed at a given location, the value of L_{50} can be extrapolated from observable salinity gradients, thus allowing values of L_{50} exceeding h or values of ψ less than 0.5. The dimensionless stratification parameter, ψ, can be interpreted as a continuum from well mixed conditions at $\psi << 1$ to highly stratified conditions at $\psi >> 1$. By analogy with the Simpson et al. (1990) model, the temporal change in the dimensionless stratification parameter can be related to the sum of straining and mixing terms, as described in greater detail in MacDonald (2003).

4.0 Results

4.1 Integrated Mixing Measurements at the Anchor Station

The integrated influence of mixing within the estuary can be assessed by comparing the distribution of the tidal-cycle integrated landward and seaward directed salt fluxes as observed at the anchor station. In Figure 5, the fluxes are binned with respect to salinity and summed independently for each of the floods and ebbs through the tidal cycle. Positive values of salt mass represent landward-directed motion and negative values represent a flux of salt in the seaward

direction. Salt flux was calculated incrementally throughout the tidal cycle, adjusting for channel width based on an estimated lateral profile derived from a nautical chart. The seaward and landward directed salt fluxes balance to within 2% through the entire tidal cycle, suggesting that this two-dimensional treatment of the observations is a good representation of conditions across the channel at the anchor station.

Salt mass enters the upstream section of the estuary at high salinities, but exits across a range of lower salinities, indicating that saline water is mixed with outgoing fresh water somewhere landward of the anchor station. Approximately 50% of the total landward salt flux occurs at S>27 compared with only approximately 4% of the total seaward directed salt flux. The mixing processes upstream of the anchor station dilute the salt wedge fluid approximately 2:1 and distribute the outgoing salt flux across a wide range of salinities. The mean salinity of the landward directed salt flux is 24.5 with a standard deviation of 5, while the mean salinity of the seaward directed salt flux is 12.6 with a standard deviation of 8. This asymmetry in the distributions is strong evidence that mixing, as opposed to horizontal advection induced by tidal oscillations, is the dominant mechanism responsible for removal of salt from the estuary during the ebb.

A temporal and spatial mean of the buoyancy flux calculated from the time series using Equation (1) yields a value of $(1.4 \pm 0.1) \times 10^{-5}\ m^2 s^{-3}$. This value represents a mean across the entire tidal cycle and the extent of the salinity intrusion. Note that this mixing is approximately an order of magnitude less intense that the mixing observed seaward of the front at the end of the ebb as reported by MacDonald and Geyer (2004). This is not surprising, however, since it represents an average across the entire tidal cycle, whereas the mixing calculated near the front is based only on the most intense period near the end of the ebb. Assuming an average estimated

buoyancy frequency of $N = 0.12\ \mathrm{s}^{-1}$, an estimate of the mean turbulent eddy diffusivity through the tidal cycle landward of the anchor station is approximately $K_z^{\rho} = 9 \times 10^{-4}\ \mathrm{m^2 s^{-1}}$.

In order to provide further justification that the source of the intermediate salinity water is, in fact, due to mixing, temperature-salinity profiles from the time series data were compared with a conservative mixing line. The time series profiles and the relative deviation of the water column from a conservative mixing line connecting the two endpoints of fresh, warm, river water (0 psu, 15^{O}C) with cold, saline, Georgia Strait water (28 psu, 11.5 ^{O}C) are plotted in Figure 6. With the exception of the initial flood, all water present at the anchor station appears to be the direct result of mixing fresh river water with Georgia Strait waters.

The fluxes presented in Figure 5 clearly indicate that a significant amount of mixing occurs in the upper portions of the estuary through the tidal cycle. In order to identify the dominant mechanisms in this process, the temporal and spatial variability of mixing is examined in more detail in the following sections. The time series data is examined in greater detail to determine the temporal variability and a complementary analysis of the channel transect data is used to deduce the spatial variability.

4.2 Temporal Variability

The stratification parameter, ψ, provides an integrated measure of the combined effect of mixing and straining mechanisms, both of which are dependent on the local velocity shear (Δu). The evolution of ψ and Δu through a tidal cycle as observed during the anchor station time series is plotted in Figure 7. The stratification parameter indicates that the water column is stratified throughout the tidal cycle, with stratification increasing dramatically to highly stratified conditions near the middle of each ebb tide, and conditions approaching a more partially mixed

situation during floods. Comparison with the velocity difference indicates that high shears during the later portions of the ebbs are likely responsible for limiting the increase in stratification that begins during the early portions of both ebbs. This sequence suggests that Δu initially contributes to the stratification by straining the salinity field, but ultimately limits it as the shear causes increased mixing later in the ebb. A pronounced difference between the first and second ebb is also observed. During the first ebb the increase in Δu limits ψ to a value of approximately 3.5-4, where it stays for the remainder of the ebb. On the second ebb, both Δu and ψ increase rapidly in the second hour and the stratification peaks above a value of 5. After this peak, however, the stratification drops below 3, and remains at a level more consistent with the stratification observed during the flood. This sequence suggests that, whereas sustained mixing is observed on the first ebb over a period of 2 hours, intense mixing may occur for a brief period early in the second ebb followed by a period of significantly less intense mixing. Stratification corresponding to the spatial profiles of the second ebb shown in Figure 2 are not plotted, but values of ψ are consistently between 2 and 3 for both profiles, indicating a uniform highly stratified condition.

The role of the shear in affecting stratification can be quantified in terms of the Richardson number. The relative strength of the shear and stratification may be defined either as a gradient Richardson number ($Ri_g = -\frac{g}{\rho}\frac{\partial \rho}{\partial z}\left(\frac{\partial u}{\partial z}\right)^{-2}$) or a bulk Richardson number ($Ri_B = g\frac{\Delta \rho}{\rho} L_{50}\left(\Delta u\right)^{-2}$,where Δ represents a difference across the limits of the pycnocline defined by L_{50}). A value of Ri_g at or below ¼ is typically considered a necessary condition for the onset of turbulence (e.g. Miles 1961; Howard 1961). However, turbulence in regions of weak stratification results in "neutral" mixing, where the weak gradients limit effective

contributions to the buoyancy flux. In order to focus on regions that can result in positive buoyancy flux an additional criteria of dS/dz>0.3 psu·m^{-1} was applied to the gradient Richardson number results. In order to take this into account, we define Ri_g(%), which represents the percentage of the water column that is both subcritical with respect to the local gradient Richardson number and meets the salinity gradient criteria.

Figure 8 shows profiles of Ri_g(%), and Ri_B for the time series data. The Ri_g(%) distribution, as shown in Figure 8(a), indicates an increase in mixing propensity during both ebbs, with water column percentages of 25 to 30% meeting the combined stability and stratification criteria. Note that the interfacial region, where the greatest buoyancy flux is likely to occur, rarely spans more than a third of the water column, as indicated by the stratification parameter in Figure 7. Thus, values of 15 to 30 percent and greater are significant, as they indicate that conditions are conducive to turbulent mixing across the majority of the stratified region. An additional, smaller peak is observed at the beginning of the time series, indicating a tendency for lower Richardson numbers associated with the head of the salt wedge. This peak is immediately followed by a period of high Richardson numbers as the percentage of the water column satisfying the Ri_g and dS/dz criteria drops to less than 3%. Little relaxation of the curve is seen during the second flood, where water column percentages of 15 to 20% are observed.

The Ri_B profile, shown in Figures 8(b) and 8(c), is generally consistent with the Ri_g(%) profile, with the notable exception of the later portions of the second ebb, when Ri_B values are greater than ¼, but a high percentage of the water column is observed to have subcritical Richardson numbers. This suggests that the region of active mixing has been depressed beneath the region identified by the L_{50} scale (approximately 7 psu to 21 psu).

Ri_g provides a useful indicator of when and where conditions are favorable for the generation of turbulence within the fluid. However, the amount of buoyancy flux that occurs as a result of the turbulence is highly dependent on the density gradient, hence the additional constraint on Ri_g(%) of dS/dz>0.3 psu·m^{-1}. Thus, the mean salinity gradient within the region of the water column satisfying the Ri_g(%) criteria was computed. Examination of this parameter indicates that stronger gradients are generally seen to occur during ebbs as opposed to floods (Figure 9). Note that the mean salinity gradient within the mixing region has a similar form to the stratification parameter, ψ; it indicates that the stratification is sustained during the first ebb and high, but short-lived during the second ebb.

A variant of the Richardson number, which is useful for evaluating two layer systems is the composite Froude number (e.g. Armi 1986), defined as $G^2 = F_1^2 + F_2^2$, where $F_j^2 = u_j^2 \left(g' h_j\right)^{-1}$ and the subscripts *1* and *2* refer to the upper and lower layers, respectively, h_j is the layer thickness, and $g' = g\left(\rho_1 - \rho_2\right)\rho_\circ^{-1}$ is a reduced gravity. The Froude number is often invoked in studies of highly stratified estuaries, including the Fraser River (e.g. Geyer and Farmer 1989; MacDonald and Geyer 2005).

Profiles of the individual layer Froude numbers (F_j) and composite Froude number (G) through the time series are shown in Figure 10. The flow is seen to be significantly supercritical during both ebbs, and subcritical during floods. It is interesting to note that the lower layer is observed to be the active layer until several hours into the first ebb, at which point the lower layer Froude number drops nearly to zero. Although these values increase during the second flood, the upper layer values never decrease sufficiently to allow the lower layer to again dominate the dynamics of the two-layer system. The difference in the active layer is the primary driver in differences between the two floods. Although both floods exhibit similar values of G,

the lower layer is much more active during the initial flood, with the net effect of reducing shear in the water column and driving Richardson numbers to supercritical (stable) values.

Thus far we have introduced a variety of indicators and estimators of turbulent intensity. Although none of these parameters are completely predictive on an independent basis, their collective analysis can be used to understand the evolution of the turbulent field during various phases of the tidal cycle. This analysis is presented below.

Temporal Evolution of the Salt Wedge: Initial Flood

During the initial flood, mixing rates are likely small, as supported by the plots of Ri_g(%), and Ri_B (Figure 8), which indicate a weakly stratified and stable water column. Stratification is approximately constant during this period at values that are low relative to the range of values observed through the tidal cycle, indicating the presence of a significant quantity of mixed water (Figure 7). The T-S diagram shown in Figure 6, however, indicates that the mixed water observed during the initial flood is not the result of local mixing processes. Instead, a third water mass is contributing to mixed water. This is most likely warm, brackish water from the shallow regions adjacent to Sand Heads, that moves in on the advancing tide.

First Ebb

The interaction of dynamic processes during the first ebb is best considered by dividing the ebb into three periods, as indicated by the vertical lines on the plots of time series data. The first hour and a half has conditions similar to the initial flood, with relatively constant stratification and low surface velocities. The plot of Ri_g(%) indicates that isolated bursts of mixing may be occurring, despite generally large values of Ri_B and subcritical values of G.

During the next hour the surface velocity begins to accelerate rapidly, driving the flow towards supercritical, and initiating an estuary-wide straining mechanism that serves to flush mixed water seaward within the upper layer, and increase the local stratification (Figure 7). During this period, mixing continues to be suppressed, as indicated by Ri_B values that are maintained above ¼. As the value of Ri_B drops below ¼ the remainder of the ebb, mixing expands across the pycnocline, stemming the increase in stratification. The nearly constant value of the stratification parameter for the next two hours suggests equilibrium between the rates of mixing and straining. High values of $Ri_g(\%)$ suggest that this equilibrium supports sustained mixing during this period.

Second Flood

The last hour of the ebb, and first hour of the second flood are characterized by a decrease in stratification, representing an adjustment due to significant changes in Δu , similar to that observed during the first ebb. In this case, straining begins to decrease with Δu , but intense mixing is maintained until the pycnocline begins to broaden (Figure 8a). Eventually, a new equilibrium is established at stratification levels similar to the initial flood. Mixing continues through the flood, driven by shears that never fall below 1 $m \cdot s^{-1}$, maintaining subcritical bulk Richardson numbers. Mixing decreases, however, due to weakening gradients within the turbulent region (Figure 9). Although the salinity structure during the second flood looks qualitatively similar to the first, as seen in Figure 4, the structure observed during the second flood cannot be attributed to the landward advection of mixed water because velocities within the region are primarily directed seaward as shown by the dashed line in Figure 4. The mixed water must be produced by mixing occurring at or landward of the anchor station. This is consistent with the temperature-salinity analysis, which shows that mixing during the second flood adheres

to a conservative mixing line (Figure 6a). This mixed fluid is likely the product of mixing processes similar to those observed on the previous ebb at sites landward of the anchor station.

Final Ebb

The dynamics of the salt wedge evolve quickly during the early hours of the final ebb, as competing mechanisms give way to a catastrophic decay of the salt wedge and its ultimate removal from the channel during the latter half of the ebb. Most indicators suggest an intense but short-lived burst of mixing occurring prior to hour +2. During this period, a subcritical spike occurs in the Ri_B profile (Figure 8c), and although there is no significant broadening of the turbulent region (Figure 8a), the density gradients within the turbulent region spike to the highest level observed during the entire tidal cycle (Figure 9). The profile of Ri_g(%) (Figure 8a), however, continues to increase for several hours after the apparent spike, suggesting a migration of the active turbulent region from the pycnocline downwards, consistent with the relatively weak gradients seen in Figure 9. Although the temporal frequency of the CTD casts precludes the direct estimation of buoyancy flux from observed overturns during this period, we conclude that there is sufficient evidence to suggest the presence of an intense but brief turbulent period early in the second ebb. Additionally the conditions observed at the time series location are likely indicative of conditions throughout the estuary, with the early hours of the second ebb heralding the catastrophic decay of the wedge. Much of the mixing during this period is likely focused upstream of the anchor station, as discussed in the following sections.

Intense mixing at discreet locations throughout the estuary tends to increase local, along channel gradients of salinity, allowing straining mechanisms to keep pace with mixing, and even increase stratification through the early portions of the final ebb. After +2 hours, the majority of

the mixed water is advected seaward without shears large enough to initiate significant mixing. This advection dramatically reduces the local stratification.

Approximately 1.5 to 2 hours prior to the removal of salt from the channel, the near-bottom velocities reverse, as shown in Figures 3 and 4, allowing the seaward advection of deep water for the first time since the beginning of the tidal cycle. These velocities can only account for approximately 1 km, or less than 10%, of the total wedge length, suggesting that the vast majority of the wedge must be removed through a vertical collapse, consistent with conclusions derived from Figure 5.

4.3 Spatial Variability

The spatial variability of the Richardson number during the ebb is shown by plotting Ri_g(%), similar to the plot in Figure 8. Both ebb profiles (2.3 and 3.3 hours) are shown in one panel on Figure 11 (a). A larger portion of the water column shows a propensity for mixing near the salt wedge head ($x \approx 10\,\text{km}$), and seaward of about $x \approx 5$ km, than in the intermediate region. Values of Ri_B are not shown, but are consistent with the plot in Figure 11 (a).

The composite Froude numbers for both channel profiles are shown in Figures 11 b and c. In both profiles the Froude number is close to the critical value ($G = 1$) across the majority of the region, which may indicate a feedback mechanism between accelerating upper layer velocities and mixing. However, beginning in the narrows (5 km) and progressing in the downstream direction, a distinct increase towards significantly supercritical values is observed, consistent with the supercritical values (G~2) observed during the ebb at the anchor station, as shown in Figure 10. These supercritical Froude numbers are likely reflective of a local acceleration due to the channel constriction, an acceleration that is substantially greater than in other regions of the channel. Although mixing is enhanced due to this acceleration, the length scales required to

return the Froude number to a critical value of unity appear to be on the order of several kilometers, at least, and a significant region of supercritical Froude numbers persists in the channel during this period. In this manner, regions of significantly supercritical Froude numbers ($G > 2$) may be an effective indicator of enhanced mixing processes.

Mean values of the control volume estimates of buoyancy flux during the ebb are shown in Figure 12. These values represent averages of the corrected profiles taken vertically across the entire depth, temporally across the limits of the data during the large daily ebb, and spatially within the limits of 1 km along-channel bins. The upper limits of error shown in Figure 12 represent standard error. The lower limits represent the mean of both the corrected and uncorrected profiles. A mean buoyancy flux value for all of the control volume calculations during the ebb landward of the time series location, averaged across all dimensions (space, time, and salinity), is 2.7×10^{-5} m^2s^{-3}, with estimated error bounds as shown on Figure 12. These results are consistent with the profiles shown in Figure 11, in that lower mixing activity is observed within the bend ($x \approx 6{,}000$ m), than seaward of the bend.

Spatial means of overturn scale were generated by grouping channel casts into along channel bins with a dimension of 1 km (Figure 13). The overall mean value for the channel region between 3 and 8 km from the mouth during the ebb portion of the tidal cycle was 38±4 cm. Local means of B_t are shown in the second panel of Figure 13, with a mean value of $(1.4\pm0.6)\times10^{-5}$ m^2s^{-3}. For these calculations, a buoyancy flux value was calculated for each individual displacement length, prior to averaging, using the local buoyancy frequency computed from the sorted profile. These estimates of B_t provide consistent results with the estimates of B generated from the control volume analysis within the limits of the errors associated with each method, and indicate that enhanced mixing is occurring within the 5 km bin. This location is

immediately seaward of the bend and within a channel constriction. It is also characterized by an increase of Froude numbers to supercritical values from values that are otherwise nearly critical (Figure 11), and an increase in Ri_g(%).

Geyer (1985, Figure 47) suggested that mixing during ebbs in the Fraser channel is focused near constrictions, providing visual evidence from echosounder output for four significant constrictions in the lower 20 km of the estuary. The data presented here provide quantitative support for these observations.

Another potential mixing mechanism worth consideration is the possibility of secondary circulation processes associated with the large bend in the channel at 6 km. The establishment of strong secondary circulation in the bend could force deep water southward, and up onto the shallow areas at the inside of the bend, where enhanced shears due to bottom friction could provide an efficient mechanism for mixing (Figure 14). Due to the dangers of maneuvering the research vessel in shallow water, this region was not sampled during the field study, so it is possible that the overall estimates of buoyancy flux during the ebb in the upstream channel may be underestimated.

5 Discussion

5.1 Mixing in the Fraser

The structure of the salt wedge in the Fraser River is initially established through advective processes, and subsequently modified by competing mixing and straining mechanisms. Each phase of the tide is characterized by an adjustment period on the order of 1 to 3 hours, where changes in shear trigger a change in the equilibrium between mixing and straining. Increases in shear enhance straining mechanisms, which move the system toward more highly stratified conditions, while stratification is relaxed during periods of lesser shear.

Mixing is active through the entire tidal cycle, with the exception of the initial stages of the first flood, but enhanced during ebbs. An estimate of average mixing during the later portions of the first ebb (hours –7.9 to –4.5) was accomplished using a method similar to the modified control volume method employed for the entire tidal cycle in Section 4.4. In this case, the observed outflux during the period was compared to the total influx distribution observed through –4.5 hours. Using Equation (1), and the estimated salt wedge length described above, an estimated B profile with a mean of 1.6×10^{-5} m^2s^{-3}, and a peak of 3×10^{-5} m^2s^{-3} was obtained. These values are conservative because it was assumed that all of the water mixed upstream of the anchor station during the period was advected past the anchor station, so that no mixed water remained upstream.

Observations by Geyer (1985) suggest that the salt wedge is uniform and highly stratified prior to the final mixing events that result in the ultimate collapse of the wedge. This point in time is coincident with the peak in stratification observed near hour +2, shown on Figure 7, and is consistent with the salt wedge salinity profiles shown in Figure 2. An estimated buoyancy flux profile for the second ebb was generated using an output distribution equal to the total outflux of salt observed at the anchor station after +2 hours. The input distribution required for Equation (1) was estimated using the total mass of seaward directed salt after +2 hours, and a hypothetical vertical salinity profile based on the longitudinal profiles of Figure 2 and Geyer (1985, Figure 10). This exercise suggested a peak buoyancy flux during the final collapse of the salt wedge equal to 5×10^{-5} m^2s^{-3}, with a mean value of approximately 3×10^{-5} m^2s^{-3}. These values are slightly larger than, but generally consistent with, the average buoyancy flux values observed in the upstream channel during the ebb (Figure 12).

The vast majority of the salt wedge is removed from the channel through an energetic collapse during the early portion of the final ebb. High shears, associated with the ebbing discharge, and increased within localized channel constrictions lead to this collapse, as suggested by Geyer (1985). It is likely that a similar collapse may occur during the first ebb, but the barotropic forcing mechanisms associated with the weaker ebb were insufficient to flush the remaining salt downstream to our measurement location

Given the overall estimate of mean buoyancy flux associated with the salt wedge calculated in Section 4.0, the estimates for the two ebbs presented above, and the overturn and control volume estimates of buoyancy flux during the ebb presented in Figures 13 and 14, a mean buoyancy flux value for the remaining portions of the tidal cycle (both floods in addition to the first few hours of each ebb) can be estimated. Table 1 summarizes the previous estimates, as well as the length of time for which each estimate is considered representative. The last column in table 1 is the product of this time and a representative salt wedge length. As shown on line 6 of Table 1, a mean buoyancy flux for the ebb portions of the tidal cycle is approximately $(2.2 \pm 0.8) \times 10^{-5}$ $m^2 s^{-3}$, representing approximately 6.6 hours of the tidal cycle. A representative buoyancy flux value for the remaining portions of the tidal cycle can then be estimated using the mean ebb estimate from line 6 and the tidal cycle average shown on line 1, yielding a buoyancy flux value of $(1.0 \pm 0.5) \times 10^{-5}$ $m^2 s^{-3}$.

It is likely that there is still considerable variability within the remaining 11.8 hours of the tidal cycle. For example, lower rates of buoyancy flux may be associated with the initial flood, as compared to the second flood, based on the observations of Ri_B and Ri_g at the anchor station. Nevertheless, this estimate is generally consistent with the temporal evolution of mixing presented above, and indicates that mixing processes associated with the salt wedge are

important through all phases of the tide. Although differences between buoyancy flux rates on flood and ebb may be significant, and as high as a factor of six, the mixing that occurs during floods cannot be considered negligible.

5.2 Comparisons With Other Estuaries

Many studies of estuarine dynamics have focused on partially mixed estuaries, such as the Hudson River. Although many aspects of estuarine dynamics are applicable across the wide physical spectrum of estuaries, differences in stratification can result in differences in the magnitude and timing of mixing within an estuary. In general the highest buoyancy fluxes in the Fraser channel were seen during ebbs, both locally and at critical mixing locations within the channel (e.g., channel constrictions). This is consistent with previous analyses of the temporal variation of mixing in estuaries, both in highly stratified (Partch and Smith, 1978), and partially mixed regimes (Nepf and Geyer, 1996). Previous work in the Fraser (Geyer and Farmer, 1989) also suggests that the ebb dominates contributions to the buoyancy flux, and that the most productive mixing occurred as a response to lateral constrictions in the channel.

Numerical simulations of a partially mixed estuary (MacCready and Geyer, 2001) indicate that while the maximum rates of buoyancy flux occur locally during ebbs, the flood is the most productive period of vertical salt flux due to the elongation of the isohalines and a larger area over which the weaker mixing processes present on the flood can act. This is consistent with the results of Peters(1999) who found that, across the tidal cycle, floods were the most effective period for mixing in the Hudson River Estuary, with the exception of spring ebbs. Based on the present observations, such a case is unlikely to be found in the Fraser River because the isohaline structure is substantially eroded during ebb tides, and the floods begin with a salt wedge that is considerably shorter in length than is present at the beginning of the ebb tides. A rebuilding of

the salt wedge, fed by landward advection of dense near-bottom water, occurs throughout the flood.

6 Conclusions

Diapycnal mixing plays a vital role in the dynamics of the Fraser River estuary, and is the primary mechanism responsible for the daily purge of salt from the estuarine channel during high flow, spring tide periods. The nature of the mixing climate is highly variable, both spatially and temporally. Spatial heterogeneity in mixing intensity is due primarily to variations in channel width, as described by Geyer (1985). Temporal variability is highly influenced by the strength of barotropic forcing, and initial conditions set up by prior phases of the tide. Average mixing during ebbs, primarily focused at localized channel constrictions, appears to be on the order of 2 to 6 times larger than the average mixing observed during the remainder of the tidal cycle, but mixing processes appear active and important to the system dynamics throughout the tidal cycle.

Acknowledgments. The authors thank Rocky Geyer, David Jay, and Philip Orton for their assistance during the field and analysis phases of this work. The effort was funded by Office of Naval Research grants N000-14-97-10134 and N000-14-97-10566, National Science Foundation grant OCE-9906787. This manuscript represents number 0X-XXXX in the SMAST Contribution Series, School for Marine Science and Technology, University of Massachusetts, Dartmouth.

References

Armi, L., 1986: The Hydraulics of two flowing layers with different densities. *J. Fluid Mechanics*, vol. 163, 27-58.

Chen, F., and D.G. MacDonald, Role of mixing in the structure and evolution of a buoyant discharge plume, *J. Geophys. Res.*, **111**, C11002, doi:10.1029/2006JC003563, 2006.

Farmer, D., and L. Armi, 1999: Stratified flow over topography: the role of small-scale entrainment and mixing in flow establishment. *Proc. R. Soc. London A*, vol. 455, 3221-3258.

Ferron, B, H. Mercier, K. Speer, A. Gargett, and K. Polzin, 1998: Mixing in the Romanche Fracture Zone. *J. Physical Oceanography*. vol. 28(10), 1929-1945.

Geyer, W.R., 1985: *The Time-Dependent Dynamics of a Salt Wedge.* Ph.D. Thesis, University of Washington, Seattle, Washington.

Geyer, W.R., 1988: The advance of a salt wedge front: Observations and dynamical model. *Physical Processes in Estuaries*, Job Dronkers and Wim van Leussen, eds. Springer-Verlag, Berlin,181-195.

Geyer, W.R. and G.A. Cannon, 1982: Sill processes related to deep water renewal in a fjord. *Journal of Geophysical Research,* vol. 87, 7985-7996.

Geyer, W.R., and J.D. Smith, 1987: Shear instability in a highly stratified estuary. *J. Physical Oceanography*, vol. 17(10), 1668-1679.

Geyer, W.R., and D.M. Farmer, 1989: Tide-induced variation of the dynamics of a salt wedge estuary. *J. Physical Oceanography*. vol. 19, 1060-1072.

Howard, L.N., 1961: Note on a paper by J.W. Miles. *J. Fluid Mechanics.*, vol. 10, 509-512.

Ivey, G.N. and J. Imberger, 1991: On the nature of turbulence in a stratified fluid. Part I: the energetics of mixing. *J. Physical Oceanography*, vol. 21, 650-658.

MacCready P. and W.R. Geyer, 2001: Estuarine salt flux through an isohaline surface, *Journal of Geophysical Research*, vol. 106(C6), 11629-11637.

MacDonald, D.G., Mixing Processes and Hydraulic Control in a Highly Stratified Estuary. Ph.D. thesis, MIT/WHOI, 2003-02.

MacDonald, D. G., and W. R. Geyer, Turbulent energy production and entrainment at a highly stratified estuarine front. *J. Geophys. Res.*, **109**, C05004, doi:10.1029/2003JC002094, 2004.

MacDonald, D.G., and W.R. Geyer, 2005. Hydraulic control of a highly stratified estuarine front. *Journal of Physical Oceanography*. **35**(3), 374-387.

MacDonald, D. G., L. Goodman, and R. D. Hetland, 2007. Turbulent dissipation in a near-field river plume: A comparison of control volume and microstructure observations with a numerical model, *J. Geophys. Res.*, **112**, C07026, doi:10.1029/2006JC004075.

McDougall, T.J., 1984: The relative roles of diapycnal and isopycnal mixing on subsurface water mass conversion. *J. Physical Oceanography*, vol. 14, 1577-1589.

Miles, J.W., 1961: On the stability of heterogeneous shear flow. *J. Fluid Mechanics*, vol. 10, 496-508.

Nepf, H.M. and W.R. Geyer, 1996: Intratidal variations in stratification and mixing in the Hudson estuary. *Journal of Geophysical Research*, vol. 101(C5), 12079-12086.

Orton, P.M. and D.A. Jay, Observations at the tidal plume front of a high-volume river outflow. *Geophys. Res. Letters*, **32**, L11605, doi:10.1029/2005GL022372, 2005.

Partch, E.N. and J.D. Smith, 1978: Time dependent mixing in a salt wedge estuary. *Estuarine and Coastal Marine Science*, vol. 6, 3-19.

Peters, H., 1999: Spatial and temporal variability of turbulent mixing in an estuary. *Journal of Marine Research*, vol. 57(6), 805-845.

Peters, H., M.C. Gregg, and J.M. Toole, 1988: On the parameterization of equatorial turbulence. *Journal of Geophysical Research*, vol. 93(C2), 1199-1218.

Pritchard, D.W., 1952: Salinity distribution and circulation in the Chesapeake Bay estuarine system. *J. Marine Research*, vol. 11, 106-123.

Pritchard, D.W., 1954: A study of the salt balance in a coastal plain estuary. *J.* Marine Research, vol. 13, 133-144.

Pritchard, D.W., 1956: The dynamic structure of a coastal plain estuary. *J. Marine Research*, vol. 15, 33-42.

Schijf, J.B. and J.C. Schonfeld, 1953: Theoretical considerations on the motion of salt and fresh water. *Proceedings of the Minnesota International Hydraulics Convention, 5th Congress I.A.H.R.*, 321-333

Seim, H.E. and M.C. Gregg, 1997: The importance of aspiration and channel curvature in producing strong vertical mixing over a sill. *Journal of Geophysical Research*, vol. 102(C2), 3451-3472.

Simpson, J.H., J. Brown, J. Matthews, and G. Allen, 1990: Tidal straining, density currents, and stirring in the control of estuarine stratification. *Estuaries*, vol. 13(2), 125-132.

Thorpe S.A., 1977: Turbulence and mixing in a Scottish loch. *Philos. Trans. Roy. Soc. London A*, vol. 286, 125-181.

Wesson, J. C., and M. C. Gregg, 1994: Mixing at Camarinal Sill in the Strait of Gibraltar. *Journal of Geophysical Research*, vol. 99, 9847-9878.

	Description of Estimate	Mean B ($\times 10^{-5}$ $m^2 s^{-3}$)	Hours	$\int Ldt$ [a] ($\times 10^4$ m·hour)
1	Anchor Station Tidal Cycle Average	1.4	18.4	17.0
2	Anchor Station First Ebb Estimate	1.6	3.5	3.7
3	Anchor Station Final Ebb Estimate	3.1	3.1	2.2
4	Overturn Ebb Estimate	1.4	7	-
5	Control Volume Final Ebb Estimate	2.7	3.3	-
6	Mean Ebb Estimate[b]	2.2 ± 0.8	6.6	5.9
7	Remainder Estimate (Mean)	1.0 ± 0.5	11.8	11.1

Notes: a. Integral represents product of wedge length, L, and time.
b. Mean B is average of lines 2 through 5. Remaining columns are sum of lines 2 and 3.

Table 1: Summary of buoyancy flux estimates through the tidal cycle. Lines 1, 2, and 3 are derived from the integrated anchor series flux calculations. Lines 4 and 5 correspond to the overturn and control volume analyses shown in Figures 13 and 14. The mean ebb estimate in line 6 represents the average of lines 2 through 5. The estimate for the remainder of the tidal cycle, in line 7, is derived from lines 1 and 6 so that a weighted mean of lines 6 and 7 is equal to the mean buoyancy flux estimate on line 1.

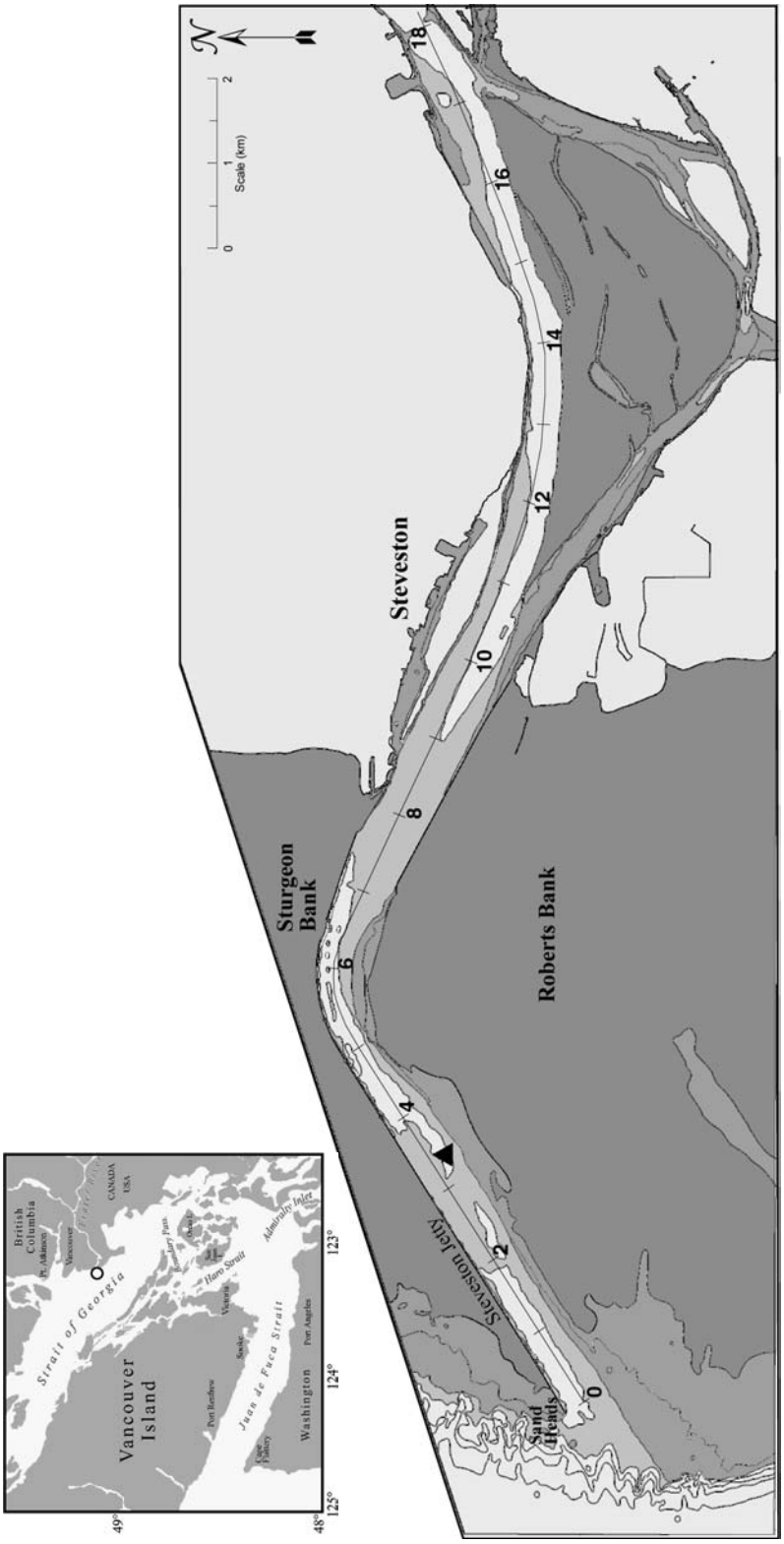

Figure 1: Locus of Fraser River estuary shown by bold circle in upper left panel. The main arm of the Fraser River at its confluence with the Strait of Georgia is shown in the main panel. Darkest shading represents banks that are submerged at high water. Remaining shading represents depth: 0-5 m, 5-10 m and greater than 10 m from dark to light. Tick marks indicate distance in kilometers from the mouth at Sand Heads. The anchor station occupied during July 3rd and 4th is located at kilometer 3.4, and shown as the black triangle.

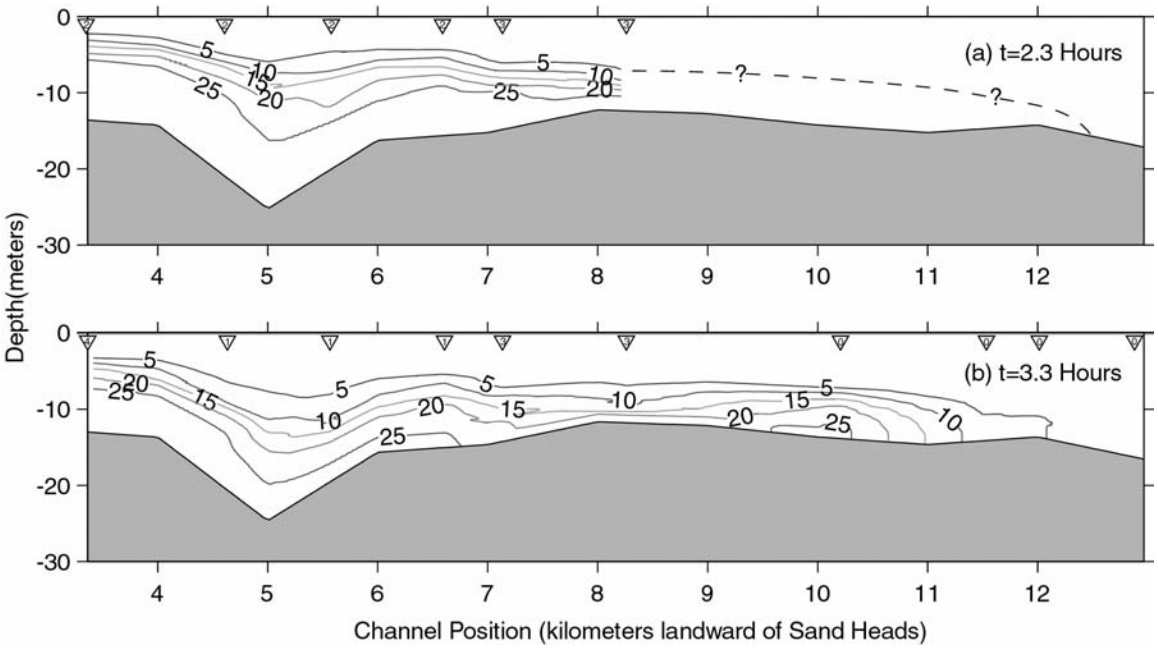

Figure 2: Composite profile of salt wedge salinity structure at 2.3 hours (top panel) and 3.3 hours (bottom panel) after high tide prior to the largest of two daily ebbs. Cast locations are indicated by the inverted triangles at the top of each panel. Numbers inside the triangles identify the date of the cast [0 - June 30; 1- July1; 2- July 2; 3- July 3; 4- July 4 (Time Series Data)]. Contours are based on an interpolation scheme normalized by channel depth.

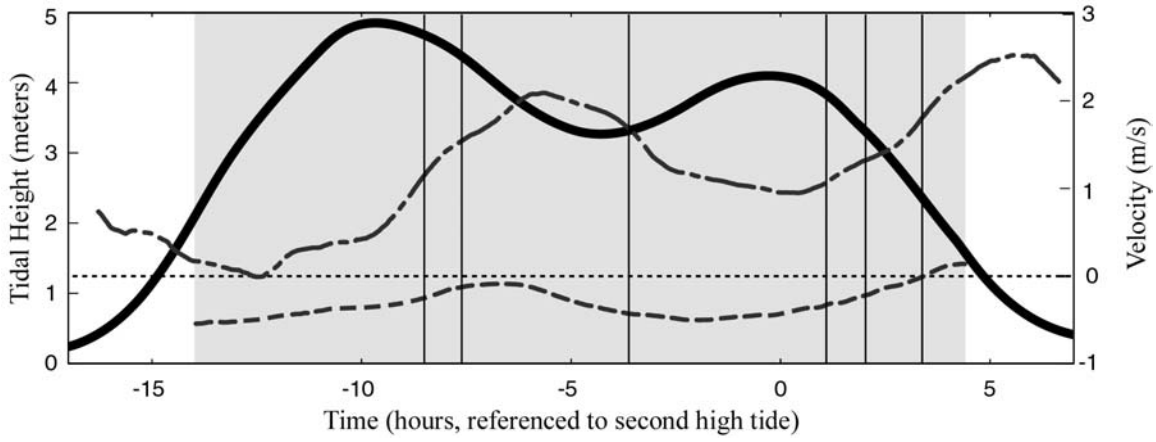

Figure 3: Tidal height (bold line), velocity 1.74 m below the surface (dash dot line, positive seaward), and velocity 2 m above the bed (dashed line, positive seaward) during occupancy of anchor station. Shaded region indicates presence of salt at anchor station. Vertical lines are for reference in comparison with other figures. Time is referenced to the second high tide.

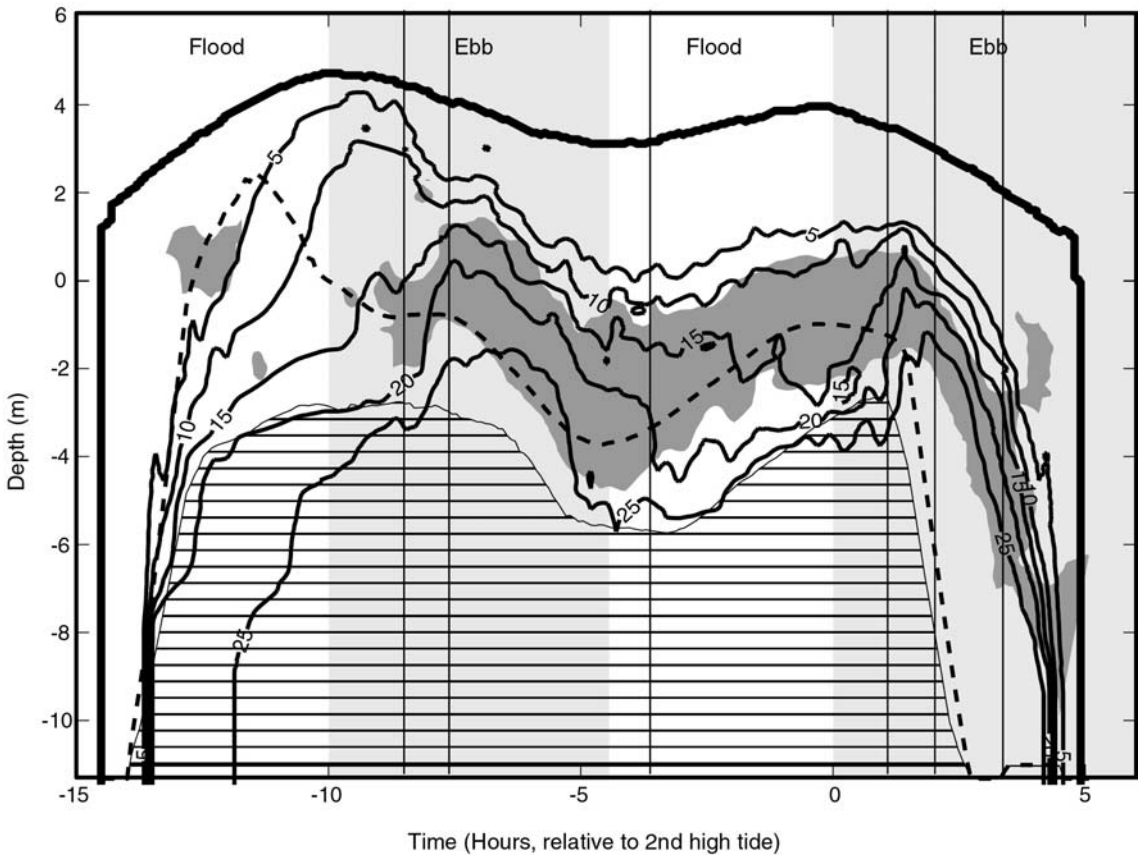

Figure 4: Contours of salinity (psu) as a function of depth and time through a tidal cycle at the anchor station. Light shaded areas represent ebb tides. Dark shaded area indicates $Ri_g < ¼$. Dashed line represents the vertical location of $u = 0$ (i.e., regions above this line are flowing seaward, and regions below the line are flowing landward). Hatched area represents the region of positive shear (i.e., velocity increasing in the landward direction away from the bed). The heavyweight line indicates the limits of the data and the surface elevation through the tidal cycle. Vertical lines are provided for reference in comparison with other figures.

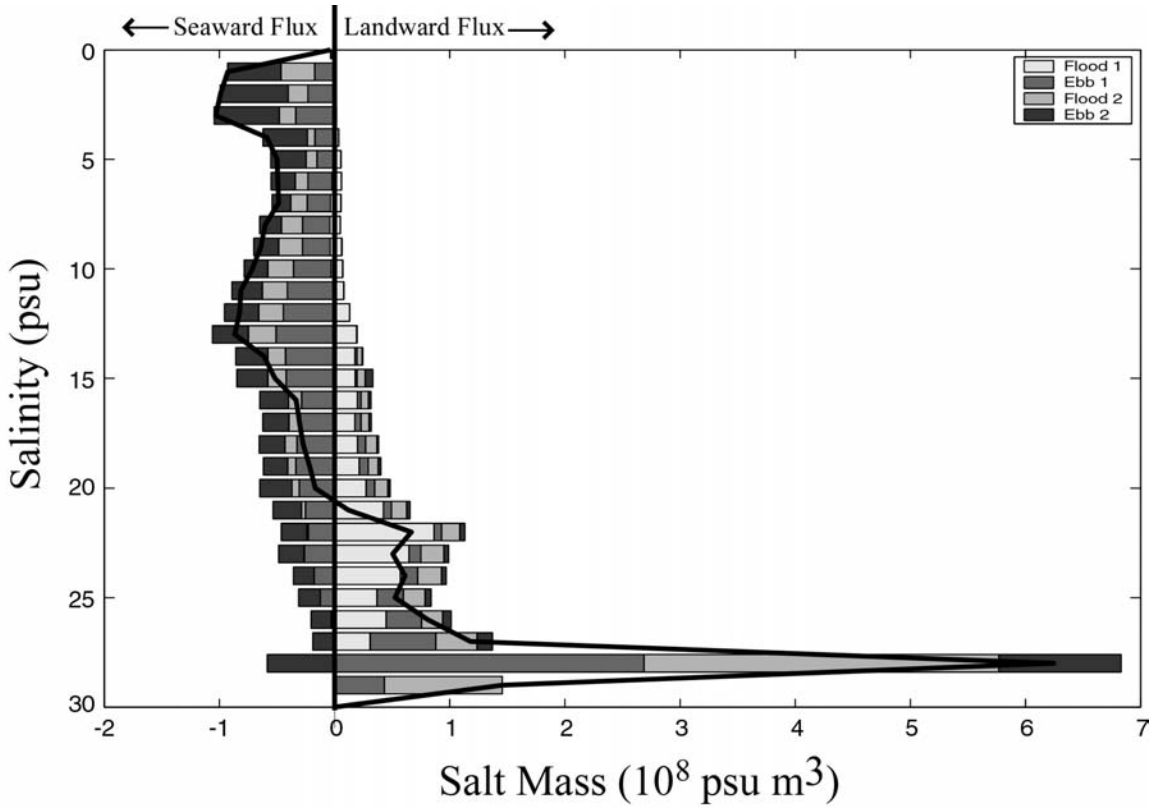

Figure 5: Bars represent total salt mass fluxed past the anchor station (3.5 km landward of Sand Heads) during a complete tidal cycle, broken into tidal phases as shown. Positive and negative values represent landward- and seaward-directed fluxes, respectively. The solid overlying curve represents the net salt mass transport for each salinity bin. The salinity scale is inverted to approximate water column depth.

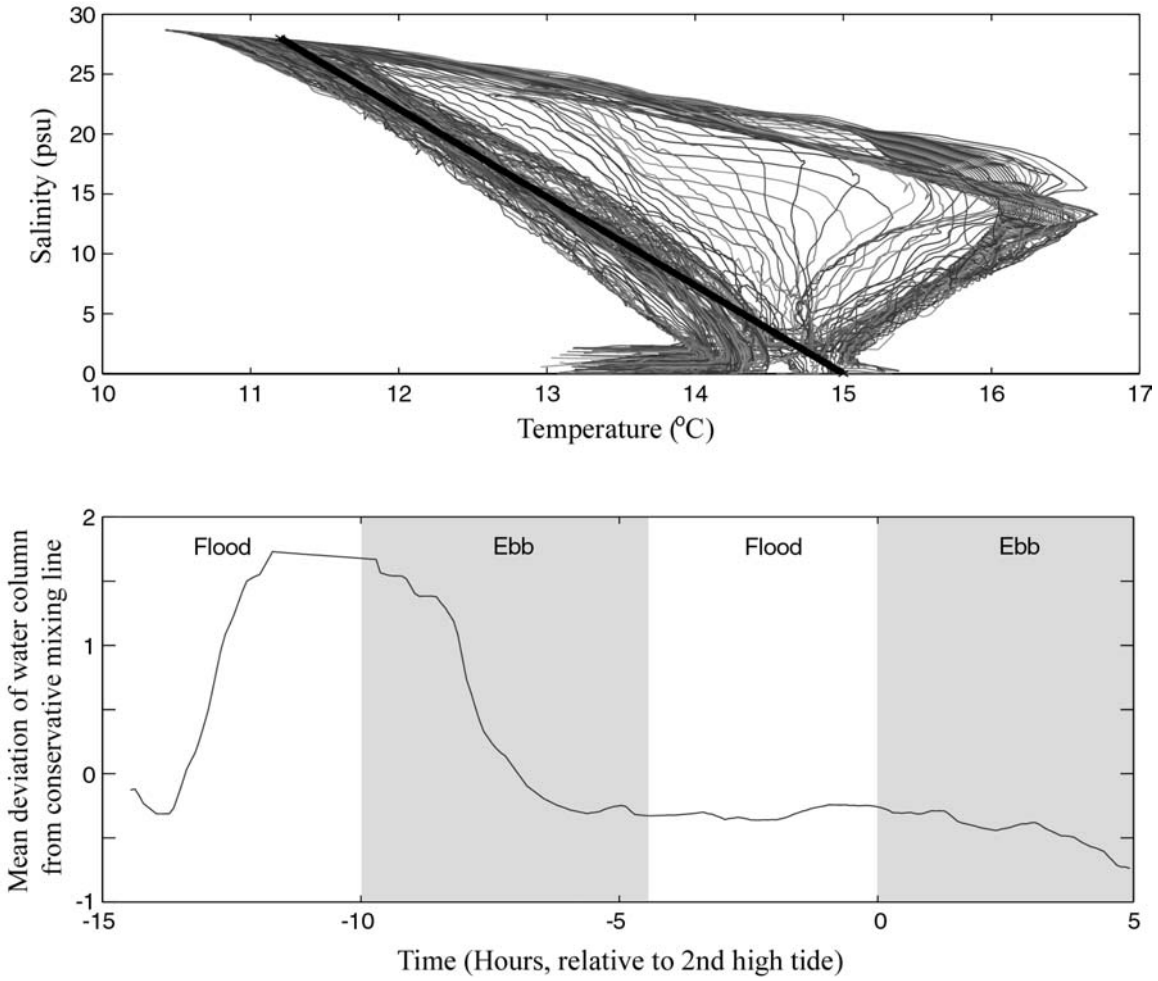

Figure 6: Temperature-salinity relationships for time series CTD casts. The upper panel represents a composite plot of all CTD casts. A conservative mixing line, connecting cold, saline Georgia Strait water with warmer, fresh river water is shown in bold. In the bottom panel, the relative mean deviation of each cast from the conservative mixing line in the upper panel is plotted.

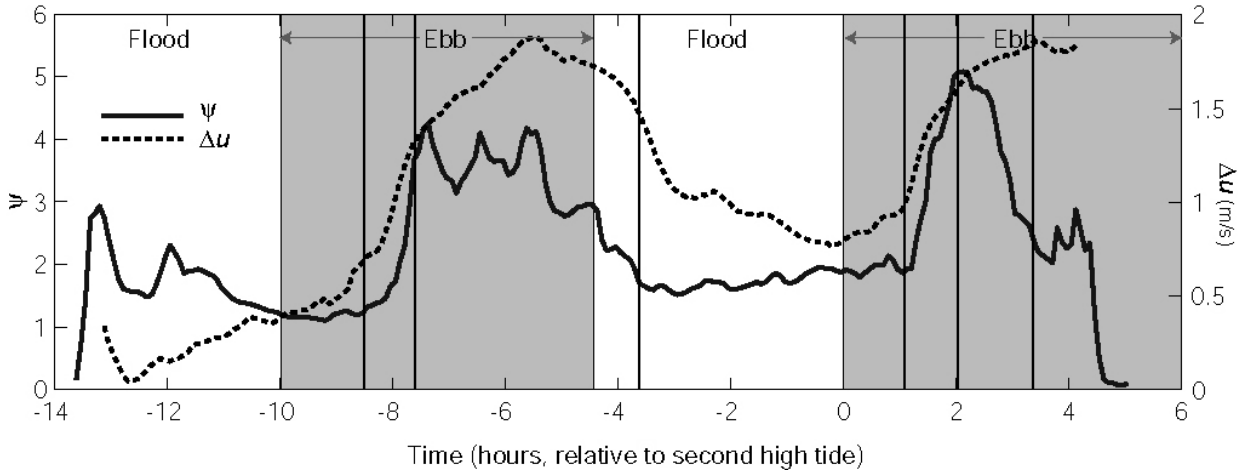

Figure 7: Stratification parameter, ψ, and velocity difference between upper and lower layer, Δu, at time series location, approximately 3.4 km landward of Sand Heads. Shaded regions represent ebb tides. Vertical lines are for reference in comparison with other figures.

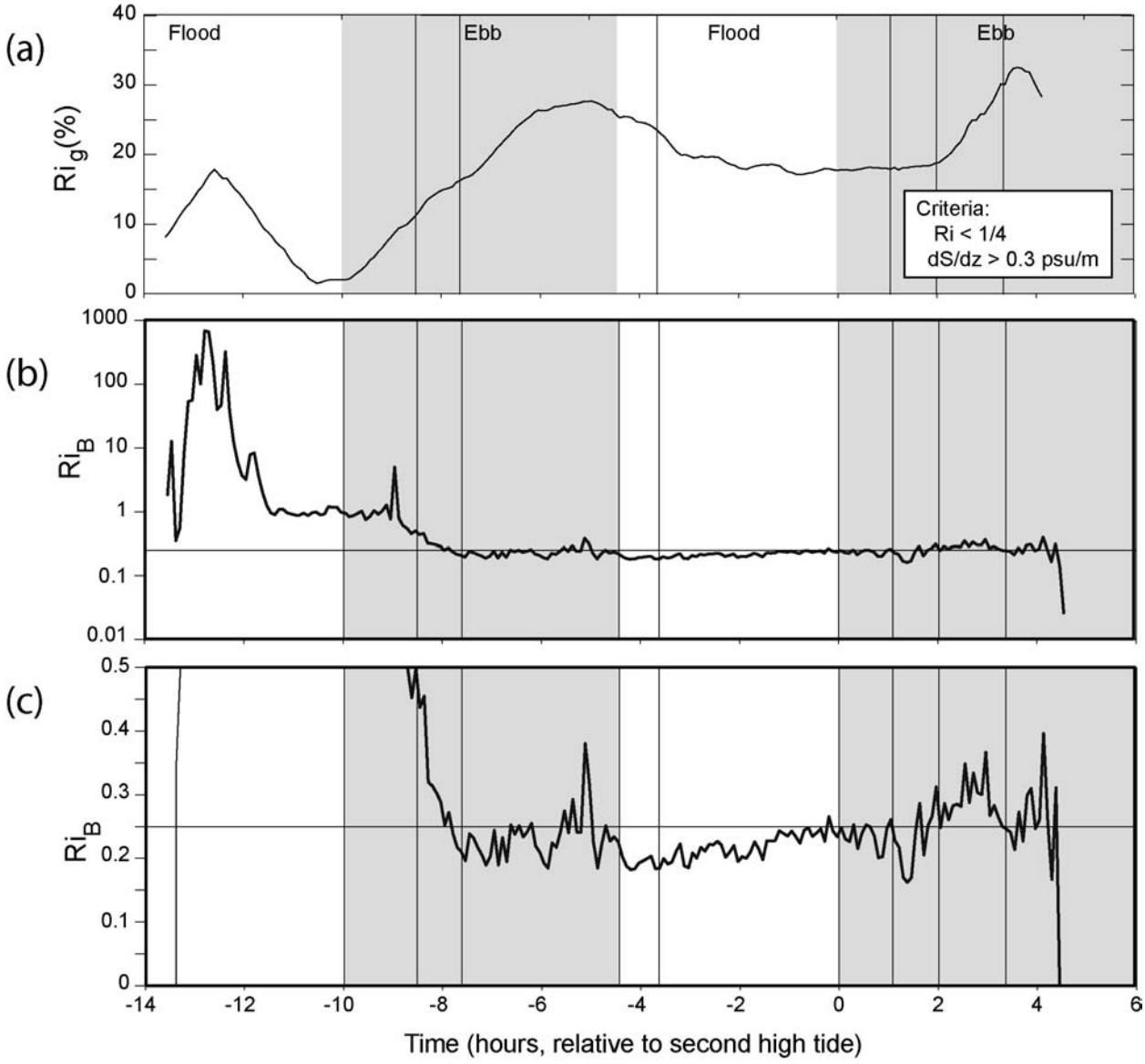

Figure 8: (a) Percent of water column with Richardson number (Ri_g) less than ¼, and $\partial S/\partial z$ greater than a minimum threshold value of 0.3 psu/m for the time series data through one complete tidal cycle (July 3-4, 2000). Panels (b) and (c) represent the bulk Richardson number across the pycnocline defined by L_{50} (approximately 7 psu to 21 psu). (b) is plotted on a log scale, and (c) on a linear scale to provide increased resolution near the value of ¼. In both (b) and (c), $Ri_B = 1/4$ is indicated by the horizontal line. Shaded areas in all panels represent ebb tides. Vertical lines are for reference in comparison with other figures.

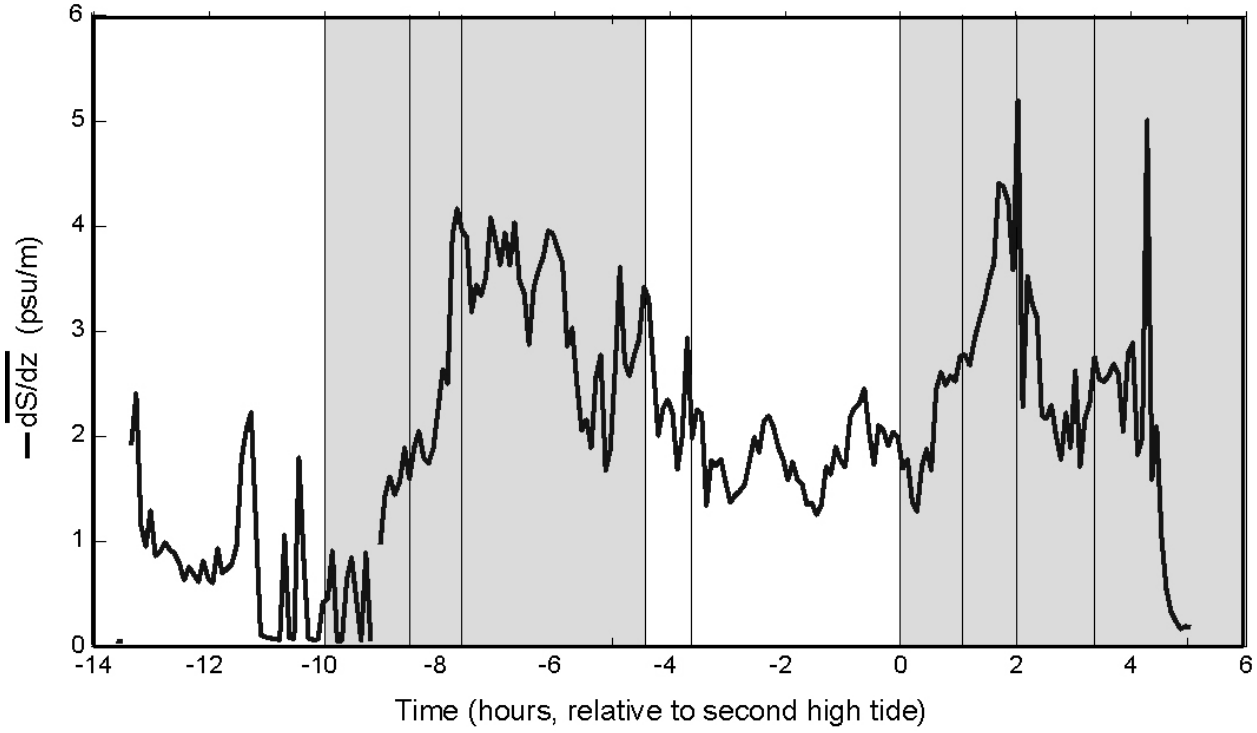

Figure 9: Mean salinity gradient within region meeting criteria for Ri_g(%).

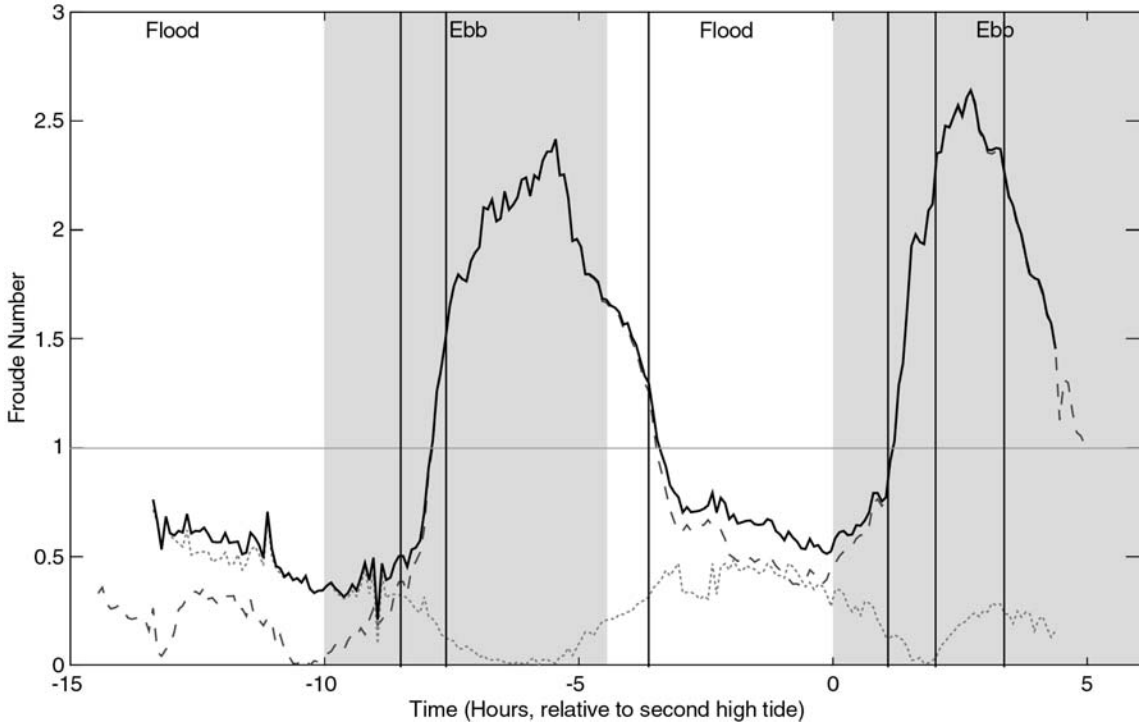

Figure 10: Internal composite Froude number (solid line), and individual layer Froude numbers (upper layer- dashed; lower layer- dotted) for the time series through one complete tidal cycle (July 3-4) at the anchor station located 3.4 km landward of Sand Heads. Shaded areas represent ebb tides. Vertical lines are provided for reference in comparison with other figures.

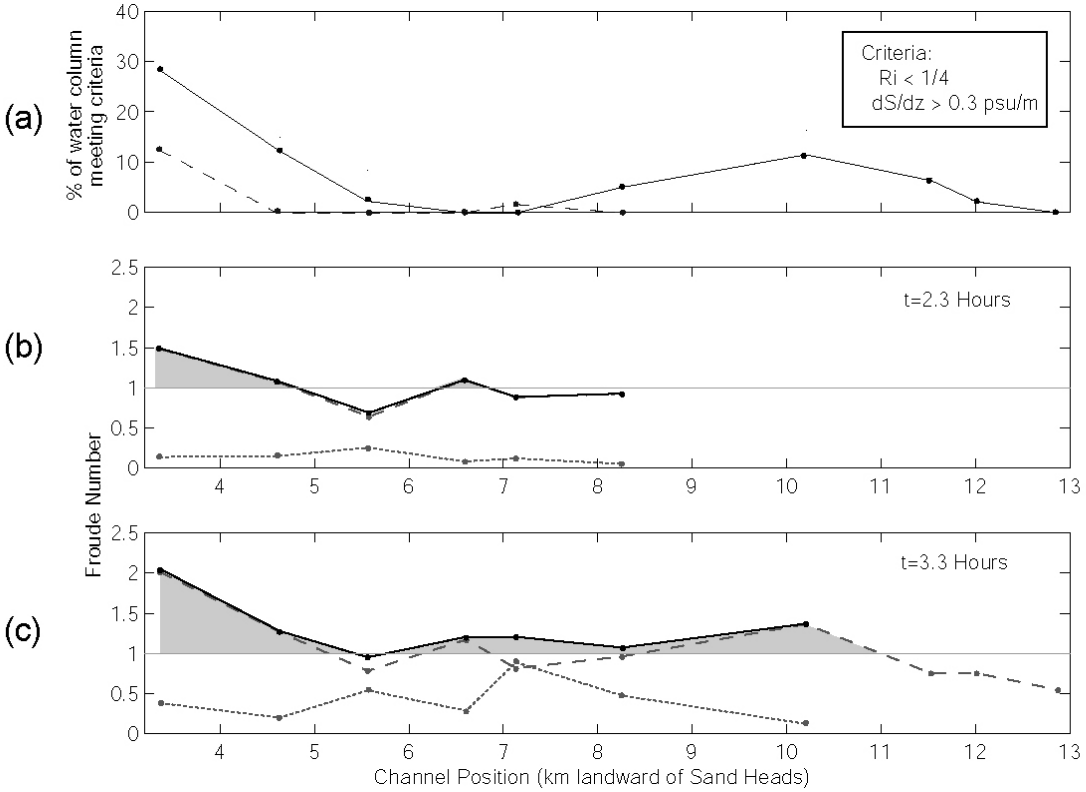

Figure 11: (a) Percent of water column with Richardson number (Ri_g) less than ¼ and $\partial S/\partial z$ greater than 0.3 psu/m, for ebb profiles at 2.3 hours (dashed line) and 3.3 hours (solid line) after second high tide. Note that the profile at 2.3 hours does not extend to the head of the salt wedge. Richardson number profiles were calculated at the cast locations indicated on Figure 2. Panels (b) and (c) represent the internal composite Froude number (solid line), and individual layer Froude numbers (upper layer- dashed; lower layer- dotted) for the ebb profiles shown in Figure 2. Froude number values were calculated at the cast locations indicated on Figure 2.

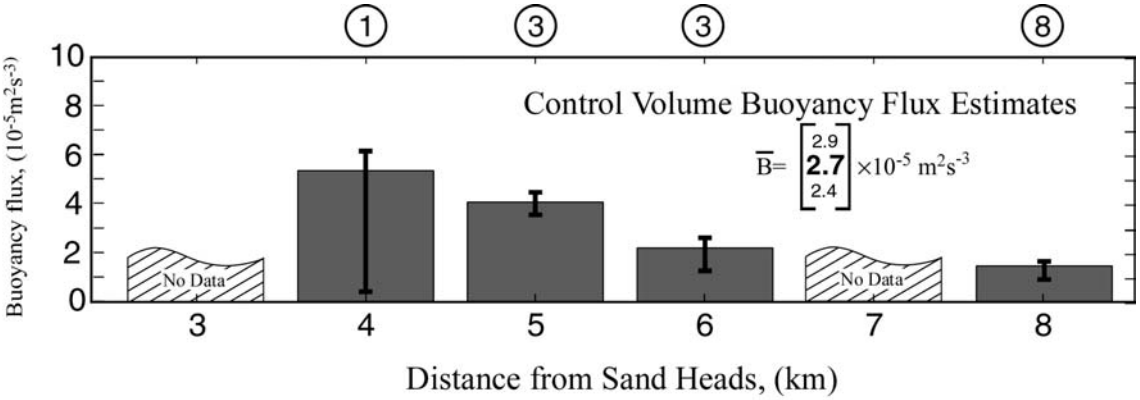

Figure 12: Spatial variability of buoyancy flux, *B*, as estimated from the control volume analysis, for observations made during the larger of the two daily ebbs (June 30 – July 4, 2000). All values represent the vertical and horizontal mean of all profiles generated within the 1 km long regions specified by the bars. The numbers in circles at the top of the panel indicate the number of profiles represented in each mean. Profiles were adjusted so that flux at the bottom was equal to zero. Errors were attributed mainly to the temporally evolving nature of the salt wedge during this period. The upper error bound represents standard error. The lower error bound represents the mean of both corrected and uncorrected profiles, as described in the text.

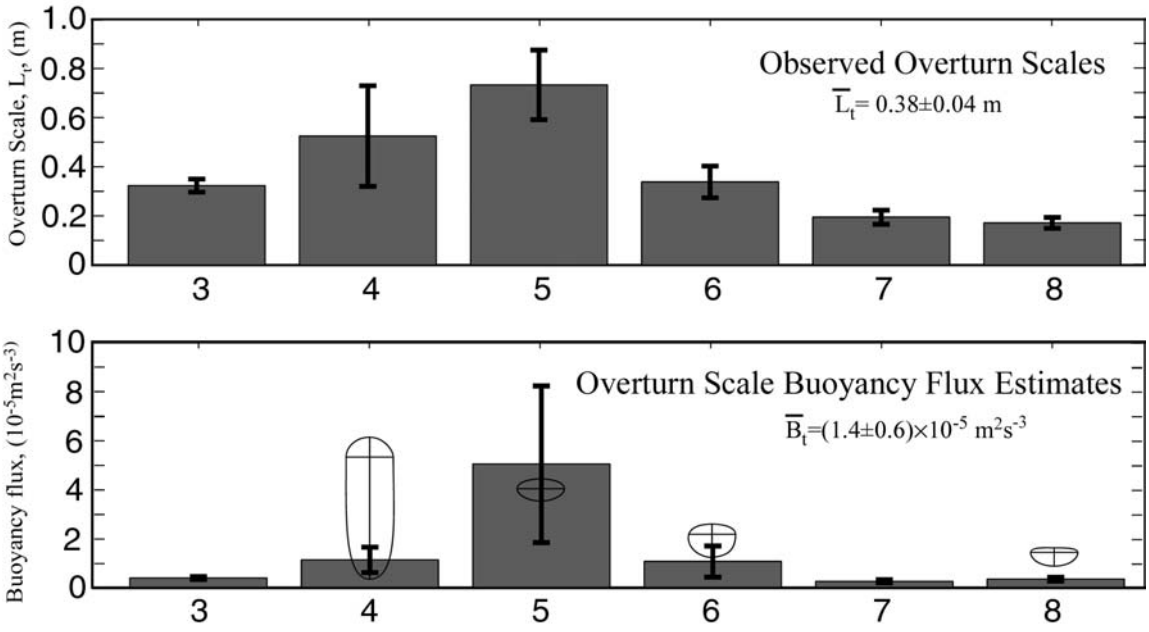

Figure 13: Spatial variability of the observed overturn scale (top panel), and buoyancy flux, B_t, as estimated from the overturn. All values represent the mean of observations from the larger of the two daily ebbs (June 30 – July 4, 2000). The error bars shown represent standard error. Crosses in the bottom panel represent the mean and error limits from the control volume method (Figure 12) for comparison.

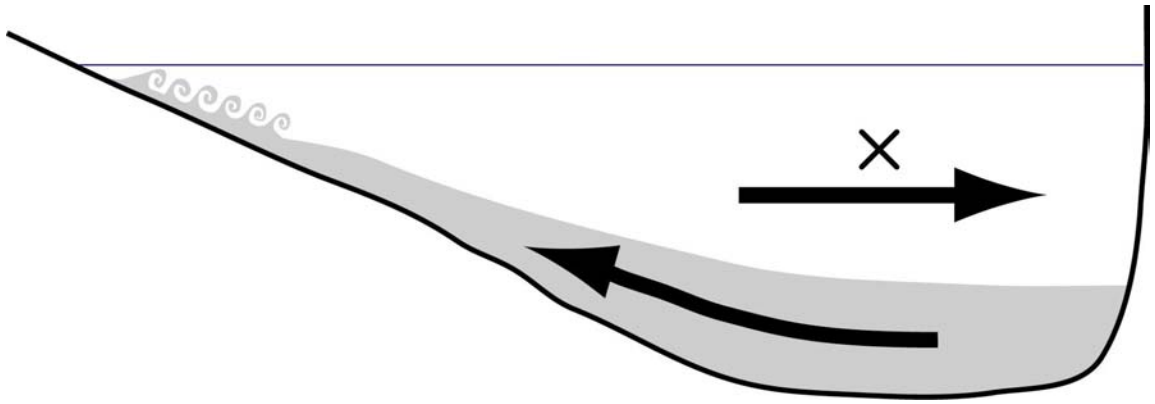

Figure 14: Schematic representation of the enhancement of boundary mixing due to secondary circulation. In this figure, the primary component of the fresh water velocity is directed into the page, and the channel is bending to the left. The induced cross-channel circulation pattern that develops is responsible for driving dense fluid up into the shallow regions of the channel located on the inside of the bend, where mixing is more intense due to the increased importance of bottom friction.